Global Journal of Engineering and Technology Advances
eISSN: 2582-5003
Cross Ref DOI: 10.30574/gjeta
Journal homepage: https://gjeta.com/

(Research Article)

Check for updates

MECHANICAL CHARACTERIZATION AND DAMAGE TOLERANCE IMPLICATIONS OF SOLID AND TRUSS NACA 6412 WING RIB CONFIGURATIONS FABRICATED WITH PETG USING FUSED DEPOSITION MODELING

Durojaye R.O.[1,*] Bashir A.F.[2], Aremo E.A [3], Ariyo F.T [3], Adebanjo O.B [3] and Odunaiya G.A [3]

[1] Projects, Planning and Strategic Development Division, Bola Ahmed Tinubu Centre for Space Transport and Propulsion, Epe Lagos Nigeria.
[2] Department of Aerospace Engineering, Faculty of Engineering, Lagos State University, Lagos, Nigeria.
[3] Rocket Systems Engineering Division, Bola Ahmed Tinubu Centre for Space Transport and Propulsion, Epe Lagos Nigeria.
* Corresponding Author

ORCID Details
Durojaye R.O: https://orcid.org/0009-0005-2009-3632
Adebanjo O.B: http://orcid.org/0009-0002-4864-5273

Global Journal of Engineering and Technology Advances, 2026, 28(03), 017–025

Publication history: Received on 18 July 2026; revised on 30 August 2026; accepted on 01 September 2026

Article DOI: https://doi.org/10.30574/gjeta.2026.28.3.0233

ABSTRACT

The structural use of Fused Deposition Modeling (FDM) printed thermoplastic components in aerospace design requires mechanical performance data at the component level, which is presently limited in the available literature. This study presents an experimental mechanical characterization of two additively manufactured NACA 6412 airfoil wing rib configurations fabricated from Polyethylene Terephthalate Glycol (PETG), carried out to assess the implications of the results for the fatigue resistance and damage tolerance of FDM printed aerospace structures. A Solid Rib with a chord length of 200.20 mm and a uniform extrusion depth of 10 mm, incorporating three circular lightening apertures, and a Truss Rib with a chord length of 180.00 mm and an extrusion depth of 3 mm, incorporating an open diagonal bracing pattern, were designed and fabricated on a Bambu Lab A1 printer from the same PETG filament stock. Five mechanical tests were carried out: static tensile testing of the PETG filament, three points flexural testing of the filament and the Solid Rib, Leeb rebound hardness testing of the Solid Rib, pendulum impact testing of the Solid Rib, and sliding wear testing of both rib configurations. Tensile testing returned a mean ultimate tensile strength of 25.24 MPa and a mean elastic modulus of 563.46 MPa for the raw filament. Three points flexural testing of the Solid Rib produced a maximum flexural stress of 19.01 MPa, a flexural elastic modulus of 210.87 MPa, a strain at maximum stress of 15.07 percent, and a fracture energy of 2.978 J. The 62.6 percent reduction in elastic modulus between the raw filament and the fabricated rib is attributed to insufficient polymer chain interdiffusion at the print parameters used rather than to a limitation of PETG as a material. Leeb hardness measurements returned a mean of 46.04 HL across three locations, with a narrow range of 2.606 HL indicating uniform surface consolidation. Pendulum impact testing returned a mean absorbed energy of 9.737 J/mm^2. Sliding wear testing showed that the Solid Rib achieved a wear resistance of 70.175 N·m/mm^3, outperforming the Truss Rib specimens at 48.001 and 41.678 N·m/mm^3. The combined results confirm that PETG retains a ductile, progressive failure mode even at sub optimal print parameters, satisfying the fundamental precondition for damage tolerance methodology to apply at the component level. Fatigue crack propagation testing and fractographic analysis were outside the scope of this study, so the damage tolerance conclusions drawn here are qualitative rather than quantitative. The study established a component level experimental baseline for FDM printed PETG wing ribs.

Keywords: Fused Deposition Modelling; PETG; NACA 6412; Wing rib; Damage tolerance; Fatigue; Additive manufacturing; Aerospace structures.

1 INTRODUCTION

The structural integrity of aerospace vehicles depends on the ability of load bearing components to withstand complex, multi axial stress states across service lifetimes that often span tens of thousands of flight hours. Wing ribs are central to this integrity. As transverse structural members, they maintain the aerodynamic contour of the lifting surface, distribute aerodynamic pressure loads onto the primary spars, and resist the in-plane shear forces generated during manoeuvre and gust loading [1]. The design philosophy governing aerospace structural safety has moved from a Safe Life approach, in which components are retired after a fixed number of cycles regardless of condition, through Fail Safe design, to the current Damage Tolerance paradigm [2]. Under this paradigm, pre-existing flaws are accepted as a manufacturing reality, and the design objective becomes ensuring that any flaw present cannot grow to a critical size within a defined inspection interval [3]. For a material to be assessed under this framework, it must first exhibit stable, observable damage progression rather than sudden brittle failure.

Additive Manufacturing (AM) has progressed from a rapid prototyping tool to a recognized route for producing functional, load bearing aerospace hardware, driven in large part by improvements in the buy to fly ratio relative to conventional subtractive manufacturing [4]. Fused Deposition Modeling (FDM), which builds parts by extruding thermoplastic filament layer by layer, is attractive for its low capital cost and its ability to produce complex external profiles without the fixturing constraints of machining. However, the layer wise construction of FDM parts introduces pronounced mechanical anisotropy. The bond strength across adjacent printed beads and layers depends on the degree of polymer chain interdiffusion achieved during deposition, and this interlayer bond is consistently weaker than the in-plane bead strength, making it the natural site for fatigue crack initiation and propagation [5]. Without component level experimental characterization, the structural reliability of FDM parts under service loading cannot be established with engineering confidence.

Polyethylene Terephthalate Glycol (PETG) is a suitable candidate material for this kind of investigation. Its glycol modified, predominantly amorphous structure produces a ductile failure mode with an observable plastic deformation stage before fracture, in contrast to the brittle fracture typical of Polylactic Acid. It also exhibits lower moisture absorption than Nylon, which preserves dimensional stability during printing and testing [6]. These properties make PETG a technically defensible choice for a damage tolerance-oriented study of FDM aerospace structures.

The NACA 6412 airfoil was selected for this investigation. In standard NACA four digits nomenclature, this profile has a maximum camber of 6 percent of chord located at 40 percent chord, and a maximum thickness of 12 percent of chord [7]. This profile is established in the aerodynamic design of Unmanned Aerial Vehicles (UAVs) and Light Sport Aircraft, and its thickness provides sufficient material depth through the rib web to support flexural, hardness, and impact testing.

Existing literature on FDM printed wing rib structures remains limited. Dogea, Yan and Millar tested a 3D printed Polylactic Acid aircraft wing rib instrumented with strain sensors, combining finite element analysis with experimental strain measurement under multiple loading configurations [8]. Šančić and colleagues characterized composite printed materials for multirotor UAV airframe parts [9]. In a broader review of fatigue behaviour across FDM printed polymers and architectures, Shanmugam and colleagues observed that the great majority of reported fatigue datasets are derived from standardized coupon geometries rather than from functional structural components [10]. This pattern is consistent with the present review of wing rib literature specifically, and it defines the gap this study addresses. No prior study has compared two structurally distinct FDM wing rib architectures, a continuous web against an open truss configuration, fabricated from the same material under the same process conditions.

In the present study, the mechanical behaviour of two additively manufactured NACA 6412 wing rib configurations, a Solid Rib and a Truss Rib, fabricated from PETG by FDM, was investigated experimentally. Comparative analyses were carried out using static tensile testing, three-point flexural testing, Leeb rebound hardness testing, pendulum impact testing, and sliding wear testing, to assess the implications of the results for the fatigue resistance and damage tolerance of FDM printed aerospace structural components.

2 MATERIAL AND METHOD

2.1 Materials

2.1.1 Specimens

Two structurally distinct NACA 6412 wing rib configurations were designed and fabricated for this study. The Solid Rib had a chord length of 200.20 mm and a uniform extrusion depth of 10.00 mm through the full planform, with three circular lightening apertures positioned through its continuous web, decreasing in diameter from the leading edge toward the trailing edge. The Truss Rib had a chord length of 180.00 mm and an extrusion depth of 3.00 mm, with an open internal diagonal and vertical truss bracing pattern connecting the upper and lower flange members in place of a continuous web. Both geometries were derived from the standard NACA 6412 four digits coordinate equations and fabricated from the same 1.75 mm diameter PETG filament stock (S3D brand).

2.1.2 Equipment

Specimens were fabricated on a Bambu Lab A1 Fused Deposition Modeling printer using Bambu Studio as the slicing software. Static tensile and three points flexural testing were performed on an Instron 3369 Universal Testing Machine, rated to 50 kN capacity. Surface hardness was assessed with a SOONDA SKD 552 Leeb rebound hardness tester. Impact resistance was assessed with a Hounsfield Balanced Impact Machine of the pendulum type. Sliding wear behaviour was assessed on a wear testing apparatus operating on the pin on disc principle, with volumetric loss interpreted through the Archard wear relation.

2.2 Method

2.2.1 Fabrication

Both rib configurations were printed in a flat XY build orientation, with the layer interfaces stacked through the thickness of each rib. The confirmed printing parameters were a nozzle temperature of 220°C, a bed temperature of 65°C, a print speed of 300 mm/s, a layer height of 0.2 mm, a cubic infill pattern, and two wall perimeters. The filament was dried at 60°C prior to printing. The print speed used is at the upper end of the range typically applied to PETG on open frame systems, and manufacturer guidance indicates that nozzle temperature should be increased accordingly at higher print speeds to maintain sufficient melt flow for interlayer bonding [11]. The 220°C nozzle temperature used here sits at the lower boundary of the commonly reported PETG printing window, so the combination of high deposition speed and moderate thermal input was expected to reduce the time available for polymer chain interdiffusion across bead boundaries.

2.2.2 Static Tensile Test

Two specimens of raw PETG filament, each of 2 mm circular cross section and 30 mm gauge length, were tested to fracture on the Instron 3369 at a constant crosshead displacement rate. The continuous load extension response was used to derive the tensile stress strain curve for each specimen, from which the ultimate tensile strength, elastic modulus, and strain at maximum stress were extracted. The test followed the general principle of uniaxial tensile loading described in ASTM D638-22 but did not comply with the standard's dog bone specimen geometry, since the material tested was raw filament wire [12]. The results are accordingly treated as material level reference data specific to the filament as supplied.

2.2.3 Three Point Flexural Test

Flexural testing was carried out on the Instron 3369 configured in a three-point bending arrangement, following the general method described in ASTM D790-17 [13]. Three specimens were tested: two raw PETG filament lengths, and one section cut from the Solid Rib, with cross sectional dimensions of 9 mm by 16 mm at the point of loading. Each specimen was supported on two fixed lower anvils while a central loading nose descended to apply a bending load at mid span until fracture. The load deflection output was used to calculate the maximum flexural stress, the flexural elastic modulus, the flexural stress at break, the energy absorbed to fracture, and the strain at maximum stress. The Truss Rib was not tested in flexure, since its 3 mm extrusion depth and open truss interior would not have provided a continuous, measurable bending response on the available fixture.

2.2.4 Leeb Rebound Hardness Test

Three Leeb rebound hardness measurements were taken at separate locations across the face of the Solid Rib using the SOONDA SKD 552 tester. The Leeb method is standardized under ISO 16859-1 for metallic materials [14]; its application here to a PETG thermoplastic specimen is a methodological adaptation, and the resulting HL values are treated as relative indicators of surface consolidation rather than as values on an absolute hardness scale. The Truss Rib was not tested, since its thickness and mass beneath the impact point were insufficient to avoid rigid body deflection during measurement.

2.2.5 Pendulum Impact Test

Impact testing was performed on the Solid Rib using the Hounsfield Balanced Impact Machine. The pendulum hammer was released from a fixed height and struck the specimen at the lowest point of its arc, and the energy absorbed during fracture was read from the calibrated dial scale in J/mm^2. Three separate readings were taken to assess repeatability. The Truss Rib was not tested, since its thin, open section would have offered negligible resistance at the energy level available from this machine.

2.2.6 Sliding Wear Test

Wear testing was performed on three specimens, two from the Truss Rib, designated A1 and B1, and one from the Solid Rib, designated Frame. Each specimen was weighed before and after sliding contact against a counter surface under a defined normal load and sliding distance. The gravimetric weight loss was converted to a volumetric loss using the density of PETG, approximately 1.27 g/cm^3 [18], and the specific wear rate and wear resistance were calculated following the Archard wear relation, in which volumetric material loss is proportional to the applied normal load and sliding distance, and inversely proportional to the hardness of the wearing surface [15]. This was the only test applied to both rib configurations.

3 RESULTS AND DISCUSSION

3.1 Static Tensile Test

The tensile properties of the raw PETG filament are presented in **Table 1**. Specimen 1 returned an ultimate tensile strength of 26.37 MPa and an elastic modulus of 643.09 MPa, while Specimen 2 returned 24.12 MPa and 483.82 MPa, giving mean values of 25.24 MPa and 563.46 MPa. The difference in modulus between the two specimens, approximately 28 percent relative to the mean, is larger than would typically be expected from the same filament spool, and most plausibly reflects the sensitivity of a thin, 2 mm diameter wire specimen to small misalignments in the wedge action grips rather than genuine material inhomogeneity. With this caveat noted, the mean values are taken as the best available estimate of the filament's axial response. The mean ultimate tensile strength is consistent with the lower end of the range reported for FDM printed PETG under optimized conditions [10], and both values are lower than typical injection moulded PETG datasheet figures, of the order of 50 MPa yield strength and 2100 MPa modulus, reflecting differences between a drawn filament wire and a consolidated moulded specimen [18]. The mean strain at maximum stress, 9.11 percent, confirms that the filament exhibits measurable ductility prior to failure, consistent with the material selection rationale for a damage tolerance-oriented study.

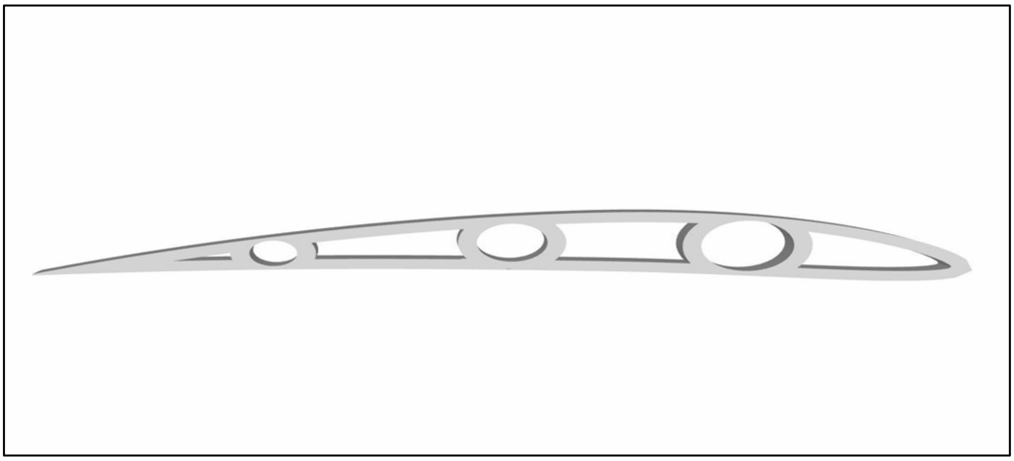

Figure 1: Solid Rib specimen — NACA 6412 airfoil profile, PETG FDM printed.

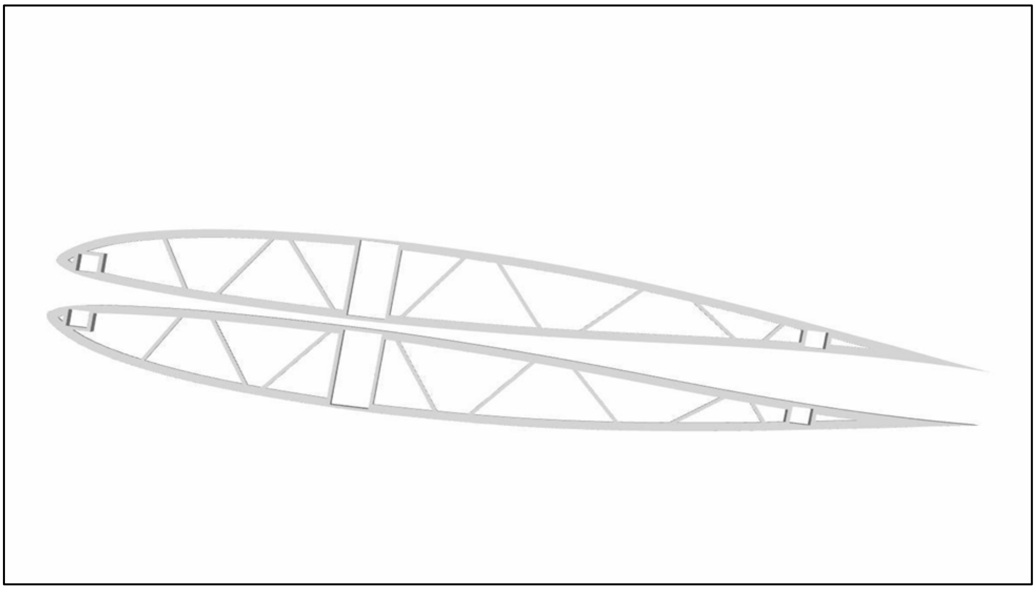

Figure 2: Truss Rib specimen — NACA 6412 airfoil profile, PETG FDM printed

Table 1: Static tensile test results for PETG filament specimens.

Specimen	UTS (MPa)	Elastic Modulus (MPa)	Strain at Max Stress (mm/mm)
1	26.37	643.09	0.068
2	24.12	483.82	0.114
Mean	25.24	563.46	0.091

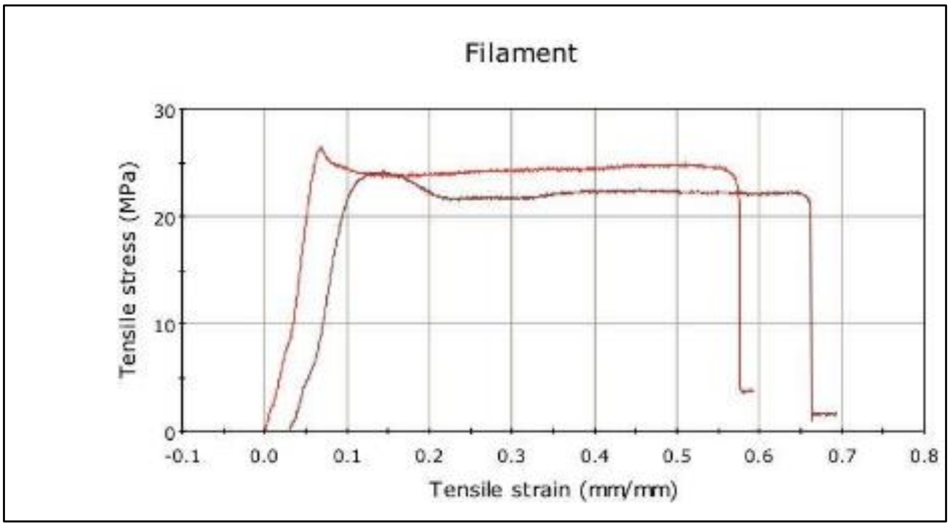

Figure 3: Tensile stress-strain curves for PETG filament specimens 1 and 2.

3.2 Three Point Flexural Test

Flexural results for the filament specimens and the Solid Rib are presented in **Table 2**. The Solid Rib returned a maximum flexural stress of 19.01 MPa, a flexural elastic modulus of 210.87 MPa, a strain at maximum stress of 15.07 percent, and an energy absorbed to fracture of 2.978 J. The most structurally significant finding is the reduction in flexural elastic modulus relative to the filament baseline. At 210.87 MPa, the Solid Rib's stiffness is reduced by approximately 62.6 percent relative to the tensile modulus of the raw filament, and by approximately 65 percent relative to the flexural modulus of Filament Specimen 2. This reduction is attributed to insufficient polymer chain interdiffusion across the inter bead and inter layer boundaries at the print speed and nozzle temperature combination used, rather than to any inherent limitation of PETG as a structural material [5,4]. Despite this stiffness reduction, the Solid Rib's post yield behaviour was not brittle. The maximum load of 273.81 N was followed by a progressive reduction to 187.31 N at fracture, a load retention of 68.4 percent, absorbed across an extension of 15.333 mm. This progressive, energy absorbing failure is the behaviour expected of an amorphous thermoplastic with a measurable plastic zone at the crack tip, and it confirms that PETG retains its ductile character even when fabricated at these print parameters. The maximum flexural stress recorded is lower than the 39 to 46 MPa range reported for FDM PETG under optimized print parameters in the literature [10], which is consistent with the print speed and temperature combination used here rather than with any material limitation. The Truss Rib was not tested in flexure, for the geometric reasons stated in Section 4.2.

Table 2: Three-point flexural test results for PETG filament and the Solid Rib.

Specimen	Max Flexural Stress (MPa)	Stress at Break (MPa)	Flexural Modulus (MPa)	Strain at Max Stress (mm/mm)	Energy to Fracture (J)
Filament 1	9.33	6.07	N/A	0.005	0.0007
Filament 2	17.87	14.85	601.89	0.049	0.0148
Solid Rib	19.01	13.01	210.87	0.151	2.978

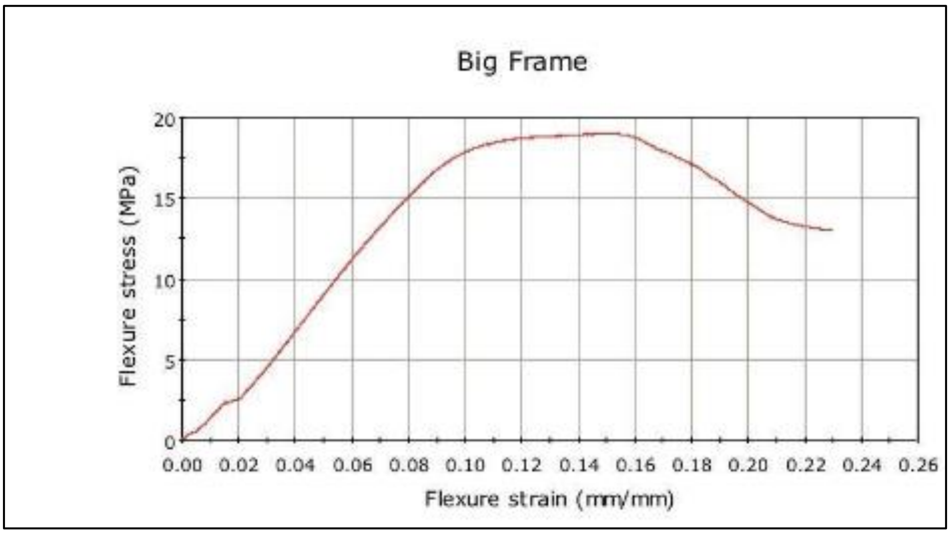

Figure 4: Flexural stress-strain curve for the Solid Rib under three-point bending.

3.3 Leeb Rebound Hardness and Pendulum Impact Test

Hardness and impact results for the Solid Rib are presented in **Table 3**. The three Leeb hardness readings ranged from 44.724 to 47.330 HL, giving a mean of 46.04 HL and a narrow range of 2.606 HL. Across three spatially distinct points on a layer wise fabricated polymer surface, this level of variation is narrow and indicates a reasonably uniform surface consolidation. As noted in Section 4.2, the Leeb method is standardized for metallic materials, and no validated conversion between Leeb HL and other polymer hardness scales, such as Shore D, currently exists for PETG; published FDM PETG Shore D values in the region of 73 to 76 D under optimized parameters [16] cannot therefore be compared directly to the values obtained here. Within this boundary, the observed uniformity suggests that no zone of significantly reduced surface consolidation was present at the outer face of the Solid Rib, which is a favourable indicator against obvious surface level fatigue crack initiation sites, although it does not rule out reduced bond quality within the rib interior, which is more directly reflected in the flexural modulus reduction reported above.

The three pendulum impact readings were 8.521, 10.275 and 10.416 J/mm^2, giving a mean of 9.737 J/mm^2 and a range of 1.895 J/mm^2. The close agreement between the second and third readings suggests repeatable measurement at those locations, while the lower first reading may reflect a local material condition or a minor difference in specimen alignment during that strike. A direct comparison of these values to standard Charpy or Izod impact data reported in the literature was not possible, since that comparison requires the specimen cross section at each impact point, which was not recorded for this test. All three readings nonetheless produced measurable, non trivial energy absorption prior to fracture, consistent with the ductile, energy absorbing failure character observed in the flexural test rather than with instantaneous brittle fracture. The Truss Rib was not tested for hardness or impact, for the geometric reasons stated in Section 4.2.

Table 3: Leeb rebound hardness and pendulum impact test results for the Solid Rib.

Measurement	Leeb Hardness (HL)	Impact Energy (J/mm^2)
1	46.056	8.521
2	44.724	10.275
3	47.330	10.416
Mean	46.04	9.737
Range	2.606	1.895

3.4 Sliding Wear Test

Wear results for the Truss Rib specimens (A1, B1) and the Solid Rib specimen (Frame) are presented in **Table 4**. The Solid Rib recorded the highest wear resistance of the three specimens, at 70.175 $N{\cdot}m/mm^3$, against 48.001 $N{\cdot}m/mm^3$ for A1 and 41.678 $N{\cdot}m/mm^3$ for B1, a superiority of approximately 46 percent over the better performing Truss Rib specimen. The volumetric loss values were derived from the measured gravimetric weight loss using an assumed PETG density; the relative ranking between specimens is unaffected since the same density factor was applied consistently across all three, although the absolute specific wear rate and wear resistance figures are best treated as internally comparable values rather than as absolute tribological constants. It is also noted that specimen B1 was subjected to a lower combined normal load and sliding distance than A1 and Frame, so its specific wear rate is not directly comparable to the other two without accounting for this difference in test conditions.

This difference in wear performance is interpretable through the Archard wear relation [15]. The Solid Rib presents a continuous, fully consolidated polymer face to the counter surface, distributing the applied normal load across a comparatively large contact area. The Truss Rib, with its open internal architecture, presents a structurally discontinuous contact geometry in which contact is limited to the thin outer flanges and the exposed ends of the truss members, producing a higher local contact pressure and accelerating material removal from those zones. This is consistent with findings in the FDM PETG tribology literature. Ranganathan et al. (2020) reported that the wear resistance and friction behaviour of neat PETG improve directly with infill density, with more structurally continuous, higher-density internal architectures consistently outperforming more open, porous ones under sliding contact [19]; Mahesh et al. (2024) observed a comparable structural-continuity effect in PETG/SCF/OMMT nanocomposites, where higher effective contact density likewise improved wear performance relative to more porous geometries [17]. As the only test applied to both rib geometries, the wear result provides the sole direct geometric comparison in this dataset, and it implies, qualitatively, that the Solid Rib geometry presents a more conservative surface stress environment under repeated contact loading, a factor relevant to fatigue crack initiation resistance. Confirming this relationship quantitatively would require surface roughness measurement and controlled fatigue testing at varying roughness levels, which were outside the scope of the present study.

Table 4: Sliding wear test results for the Truss Rib and Solid Rib specimens.

Specimen	Rib	Initial Mass (g)	Final Mass (g)	Mass Loss (g)	Volume Loss (mm^3)	Specific Wear Rate (mm^3/Nm)	Wear Resistance ($N{\cdot}m/mm^3$)
A1	Truss	18.3547	18.3209	0.0338	12.500	0.02083	48.001
B1	Truss	17.9175	17.9026	0.0149	5.5185	0.02399	41.678
Frame	Solid	18.3010	18.2749	0.0231	8.550	0.01425	70.175

4 CONCLUSION

This study has demonstrated the influence of Fused Deposition Modeling process conditions on the mechanical performance and damage tolerance relevant behaviour of PETG wing rib structures for aerospace applications. The fabrication process, specifically the combination of a 300 mm/s print speed and a 220°C nozzle temperature on an open frame system, was the primary determinant of the Solid Rib's structural performance. The flexural elastic modulus of the fabricated Solid Rib, 210.87 MPa, represented a 62.6 percent reduction relative to the tensile modulus of the raw PETG filament, 563.46 MPa, a reduction attributed to insufficient polymer chain interdiffusion at the thermal energy and dwell time available under these print settings rather than to any inherent limitation of PETG as a structural material.

Despite this stiffness reduction, PETG retained its characteristically ductile, progressive failure behaviour under both bending and impact loading. The Solid Rib sustained a flexural strain of 15.07 percent at maximum load, absorbed 2.978 J of energy before final fracture, and retained 68.4 percent of its peak load at the point of fracture rather than failing suddenly. The mean pendulum impact energy absorption of 9.737 J/mm² across three readings further confirmed that the fabricated structure responds to dynamic loading through measurable energy dissipation. These results confirm that PETG, even when printed at sub optimal parameters, satisfies the fundamental precondition for a damage tolerance design philosophy, in that the material deforms visibly and progressively before final failure.

The Leeb hardness test returned a mean of 46.04 HL with a narrow range of 2.606 HL, indicating reasonably uniform surface consolidation across the Solid Rib and no obvious zone of reduced surface integrity. The sliding wear test, the only test applied to both rib configurations, showed the Solid Rib outperforming the Truss Rib specimens in wear resistance by approximately 46 percent, a difference attributed to the distributed contact geometry of the continuous solid web relative to the concentrated contact geometry of the open truss architecture.

Fatigue crack propagation testing and fractographic analysis were not carried out within the scope of this study, so the damage tolerance conclusions drawn here are qualitative and precondition based rather than quantitative and life predictive. The results nonetheless establish a component level experimental baseline for FDM printed PETG NACA 6412 wing ribs that is not available from existing coupon level literature. Optimization of print speed and nozzle temperature, together with fatigue crack propagation testing and fractographic analysis of both rib geometries, are identified as the direct next steps required to advance this baseline toward a quantitative damage tolerance assessment.

STATEMENTS ON COMPLIANCE WITH ETHICAL STANDARDS

Acknowledgments

We sincerely appreciate the Centre for Energy research and Development (CERD) Obafemi Awolowo University Ile-Ife for the use of their facilities during this research work.

Disclosure of conflict of interest

There are no conflicts of interest.

REFERENCES

[1] Megson, T. H. G. (2017). Aircraft structures for engineering students (6th ed.). Butterworth-Heinemann.

[2] Tavares, S. M. O. (2017). An overview of fatigue in aircraft structures. Fatigue and Fracture of Engineering Materials and Structures, 40(10), 1510-1529.

[3] Anderson, T. L. (2017). Fracture mechanics: Fundamentals and applications (4th ed.). CRC Press.

[4] Gibson, I., Rosen, D., & Stucker, B. (2021). Additive manufacturing technologies (3rd ed.). Springer Nature.

[5] Afrose, M. F., Masood, S. H., Iovenitti, P., Nikzad, M., & Sbarski, I. (2016). Effects of part build orientations on fatigue behaviour of FDM-processed PLA. Progress in Additive Manufacturing, 1(1-2), 21-28.

[6] Callister, W. D., & Rethwisch, D. G. (2020). Materials science and engineering: An introduction (10th ed.). Wiley.

[7] Abbott, I. H., & Von Doenhoff, A. E. (1959). Theory of wing sections: Including a summary of airfoil data. Dover Publications.

[8] Dogea, R., Yan, X. T., & Millar, R. (2023). Testing and evaluation of the structural performance of a 3D-printed polylactic acid aircraft wing rib. Discover Mechanical Engineering, 2, Article 6.

[9] Šancić, T., Brčić, M., Kotarski, D., & Łukaszewicz, A. (2023). Experimental characterization of composite-printed materials for the production of multirotor UAV airframe parts. Materials, 16(14), 5060.

[10] Shanmugam, V., Das, O., Babu, K., Marimuthu, U., Veerasimman, A., Jeyachandran, D., & Ramakrishna, S. (2021). Fatigue behaviour of FDM-3D printed polymers, polymeric composites and architectures. International Journal of Fatigue, 143, 106007.

[11] Bambu Lab. (2024). PETG usage guide. Bambu Lab Wiki.

[12] ASTM International. (2022). Standard test method for tensile properties of plastics (ASTM D638-22).

[13] ASTM International. (2017). Standard test methods for flexural properties of unreinforced and reinforced plastics and electrical insulating materials (ASTM D790-17).

[14] International Organization for Standardization. (2015). Metallic materials, Leeb hardness test, Part 1: Test method (ISO 16859-1).

[15] Archard, J. F. (1953). Contact and rubbing of flat surfaces. Journal of Applied Physics, 24(8), 981-988.

[16] Ulkir, O. (2025). Prediction and optimization of PETG part hardness in 3D printing: A comparative study of experimental design methods. Polymers for Advanced Technologies.

[17] Mahesh, V., George, J. P., Mahesh, V., Chakraborty, H., Mukunda, S., & Ponnusami, S. A. (2024). Dry-sliding wear properties of 3D printed PETG/SCF/OMMT nanocomposites: Experimentation and model predictions using artificial neural network. Journal of Composite Materials, 57, 111-125.

[18] rigid.ink. (n.d.). PETG technical data sheet. https://devel.lulzbot.com/filament/Rigid_Ink/PETG%20DATA%20SHEET.pdf

[19] Ranganathan, S., Kumar K, S., Gopal, S., & Palanivelu, R. (2020). Enhancing the tribological properties of PETG and CFPETG composites fabricated by FDM via various infill density and annealing. SAE Technical Paper 2020-28-0429. https://doi.org/10.4271/2020-28-0429